Constraining Permeability Evolution During and After Natural Fracturing in Overpressured Shales: Implications on Basin-scale Stress and Pore Pressure Evolution

Laainam Chaipornkaew[1], Evan J. Earnest[2], Marek Kacewicz[2], and Peter J. Lovely[2]

Search and Discovery Article #42570 (2021)**
Posted May 5, 2021

*Adapted from oral presentation accepted for the 2020 AAPG Annual Convention and Exhibition online meeting, September 29 – October 1, 2020
 DOI:10.1306/42570Chaipornkaew2021

[1]Stanford University
[2]Chevron Energy Technology Company

Abstract

Most shales undergo some forms of inelastic deformation, which may include effects from compaction under increased confining pressure, with additional enhancement via horizontal tectonic stresses. Chaipornkaew et al. (EAGE 2019) proposed a mechanism that allows flow through fractured shales as a function of effective stress and pore pressure. These overpressure-driven fractures allow episodic discharge of excess fluid and consequently pressure dissipation from fractured elements via a permeability modification function that enhances flow transmissivity. This study focuses on refining this function by quantifying (1) initial permeability increases during tensile fracture formation and (2) subsequent permeability reduction due to stress-induced closure. To demonstrate the effects of permeability evolution during and after fracturing, we generate endmember realizations of Discrete Fracture Networks (DFN). We assume fracture aperture is correlated with fracture size because we model fracture at the time of formation when chemical alteration is insignificant. Stress-induced fracture behavior is modelled with a simple constitutive relation. Evolution of fracture aperture and permeability are first defined for single fractures of variable sizes and elastic moduli. Subsequently, derived relationships are applied to all fractures in the target DFN. Since, matrix permeability in shales is typically very low (~μ), we make the following assumptions. First, fracture permeability can be represented by modified (enhanced) matrix permeability. Second, DFN permeability represents DFN geometry and connectivity, which are correlated to fluid flow through the system. Third, DFN permeability can be upscaled to effective basin-scale permeability for large-size elements. The upscaled permeability reflects the permeability range representing selected DFN and elastic properties of shales. To study evolving properties of shales we built a series of synthetic models using a finite element code designed for Evolutionary Geomechanical Basin Modeling (ParaGeo). We present two fracture permeability evolution scenarios: 1. step function (base case) and 2. continuous permeability change with stress for two shale endmember scenarios: Soft Shale vs Stiff Shale (modulus 3GPa vs 30GPa). Soft Shale reveals much larger changes in permeability as compared to Stiff Shale under applied effective stress. We concluded that immediate cutoff in fracture permeability as stress and pressure condition drop below

fracturing criterion (base case scenario) may lead to incorrect rock properties and computed pore pressure in fractured elements. This may have significant implications for modeling hydrocarbon migration efficiency and expulsion from fractured shales.

Workflow to Refine Permeability Multiplication Functions

Chaipornkaew et al. (2019) proposed a mechanism that allows pressure dissipation through seal rocks as a function of effective stress and pore pressure. As fracturing criteria are satisfied, a permeability multiplier is applied to enhance fluid flow. This simple approach has the potential to model evolutionary stress and pressure in a manner consistent with permeability changes due to fracturing. This paper takes the problem one step further suggesting nonlinear stress-dependency of the multiplier to represent initial permeability increases during tensile fracture formation and subsequent permeability decreases due to stress-induced closure. We propose the new workflow (Figure 1), which utilizes feedback loops between evolutionary stress and pressure (ParaGeo's output), and upscaled permeability computed for a DFN (FracMan's output). To derive permeability modification functions, we perform the following tasks: create a series of realistic DFN, relate stress to changes in fracture aperture and permeability, calibrate with published stress and fracture permeability relations, and upscale to effective basin-scale permeability for use in evolutionary geomechanical basin models. The following sections discuss these tasks with greater details.

Discrete Fracture Network

An example of discrete fracture network (DFN) with densely spaced, sub-vertical tensile fractures with bed-bound geometry is shown in Figure 2. The DFN is designed to be analogous to several outcrop exposures (Gale et al., 2014; Dusseault, 2015; Stephenson et al., 2018). In this DFN, fractures are stochastically seeded with an exponential distributed fracture size. We express fracture size in terms of equivalent fracture radius (EQR), or the radius of a circle with the same area as the rectangular fracture with length F_L and height F_H. It is assumed that fracture aperture is correlated linearly with fracture size, a reasonable approximation as chemical alteration is minimal at the onset of fracture formation. We use cubic law to relate fracture size to fracture permeability. See Figure 2 for DFN's geometry, statistics, and histogram of initial fracture aperture and permeability. We do not attempt to model fracture growth or the evolution of DFN properties such as size, density and connectivity. In this presentation, we analyze the permeability evolution of a single DFN in which only fracture aperture evolves; however, we recognize the importance of these other attributes influencing permeability of the fracture network. Future work will focus on creating a series of DFN that represent different geologic settings and capture the inherent uncertainty of fracture network permeability for use in evolutionary geomechanical models.

Stress-Induced Aperture

We apply a constitutive relation (Bandis et al., 1983) to calculate aperture of individual fractures using Chevron proprietary workflow. Figure 3 shows permeability as a function of stress for fractures ranging in the EQR from 5 to 500 meters, for two representative endmember rocks: soft and stiff shales. Young's Modulus for these shales are constrained using laboratory characterization (Josh et al., 2012; Sone and Zoback, 2013). Then, we interpolate stress-induced aperture evolutionary relationship in both soft and stiff cases to all fractures in our target DFN according to

their size and orientation (Figure 4). The mean aperture in soft shale is reduced by almost 80% at 5Mpa applied effective stress. On the other hand, the largest fractures in the stiff shale case are closing by 20% at 5 MPa applied stress. We also model the stress-induced changes in fracture permeability as the square of changes in aperture (cubic law).

Upscaled Permeability

Because matrix permeability in shales is typically very low (~μ), we attribute permeability changes solely to changes in fractures. The added DFN permeability represents enhanced fluid flow through the system. Thus, its upscaled value is a sufficient approximation of effective permeability for large-size (~100m) elements in evolutionary geomechanical basin models.

We adopt a geometric-based upscaling approximation (Oda, 1985) where an upscaled permeability tensor is calculated by summing the effects of individual fractures weighted by their area and transmissivity, to consistently upscale individual fracture permeability into basin-scale effective permeability (Figure 5A). Although flow-based approach to permeability upscaling might better capture network connectivity, we use Oda's upscaling method because flow-based results are sensitive to grid size and generally in the same order of magnitude. Figure 5B depicts upscaled permeability from our target DFN based on two property-endmembers using geometric-based assumption: Oda_stiff_shale and Oda_soft_shale. Our modelled results (Oda_soft_member) for permeability evolution is comparable range in relation to Zhou et al. (2019)'s laboratory experiment (Figure 6).

Evolutionary Geomechanical Basin Model

To complete the workflow, we apply the permeability modification functions derived from upscaled DFN permeability back into an evolutionary geomechanical basin model. This synthetic model is motivated by an active convergent margin to represent overpressure conditions initially generated by rapid sedimentation and enhanced by compressional tectonics (Figure 7). Our evolutionary model is simulated using the finite element code ParaGeo, using a critical state poroelastoplastic constitutive formulation (Crook, 2013). This fully coupled geomechanical-fluid simulator accommodates both compaction and shear dilatancy and handles large strain accumulation through geologic time (Obradors-Prats et al., 2016).

Implications of Permeability Multiplier in Predicting Pore Pressure Evolution

Soft shale reveals much faster reduction in upscaled fracture permeability compared to stiff shale under applied effective stress (Figure 5B). While rapid permeability changes in the soft case are quite similar to Chaipornkaew et al., (2019)'s step-function multiplier, pressure and stress from the evolutionary geomechanical basin models differ significantly (Figure 8). We suggest that immediate cutoff (no closure evolution) in fracture permeability as stress and pressure condition drop below fracturing criterion may lead to incorrect rock properties and computed pore pressure in fractured elements during timestep T0 + 0.6Ma. This effect intensifies as the buildup of enclosed anomalies experiences increasing vertical overburden loads and horizontal stress in subsequent timestep (i.e. T0 + 1Ma). We are confident that modeling permeability changes

with stress evolution is theoretically more robust than without. However, validating the inherent uncertainty of fracture network permeability is critical to fully reveal implications for hydrocarbon migration efficiency and expulsion from fractured shales.

Acknowledgment

The authors thank Chevron Energy Technology Company and Three Cliffs Geomechanical Analysis Ltd for access to ParaGeo software and for permission to present this work. Funding and participation in the basin-scale inelastic deformation research is made possible through the support of the Stanford Basin and Petroleum System Modeling Group with essential advancement of fracture modeling with evolutionary geomechanical approach through an internship at Chevron Energy Technology Company.

Reference

Bandis, S. C., A. C. Lumsden, and N. R. Barton, 1983, Fundamentals of rock joint deformation: International Journal of Rock Mechanics and Mining Sciences and, doi:10.1016/0148-9062(83)90595-8.

Barnes, P. M., A. Nicol, and T. Harrison, 2002, Late Cenozoic evolution and earthquake potential of an active listric thrust complex above the Hikurangi subduction zone, New Zealand: Bulletin of the Geological Society of America, doi:10.1130/0016-7606(2002)114<1379:LCEAEP>2.0.CO;2.

Burgreen-Chan, B., K. E. Meisling, and S. Graham, 2016, Basin and petroleum system modelling of the East Coast Basin, New Zealand: a test of overpressure scenarios in a convergent margin: Basin Research, v. 28, no. 4, p. 536–567, doi:10.1111/bre.12121.

Chaipornkaew, L., M. Kacewicz, and P. J. Lovely, 2019, Basin-scale inelastic deformation: Pore pressure and stress implications, *in* 81st EAGE Conference and Exhibition 2019: doi:10.3997/2214-4609.201900946.

Crook, A. J. L., 2013, ParaGeo: A Finite element model for coupled simulation of the evolution of geological structures: Three Cliffs Geomechanical Analysis, Swansea, UK.

Dusseault, M., 2015, Geomechanical aspects of shale gas development. Keynote lecture, Eurock2013: Rock Mechanics for Resources, Energy and Environment. Kwasniewski and Lydzba, p. 39–56.

Gale, J. F. W., S. E. Laubach, J. E. Olson, P. Eichhubl, and A. Fall, 2014, Natural fractures in shale: A review and new observations: AAPG Bulletin, doi:10.1306/08121413151.

Josh, M., L. Esteban, C. Delle Piane, J. Sarout, D. N. Dewhurst, and M. B. Clennell, 2012, Laboratory characterisation of shale properties: Journal of Petroleum Science and Engineering, doi:10.1016/j.petrol.2012.01.023.

Obradors-Prats, J., M. Rouainia, A. C. Aplin, and A. J. L. Crook, 2016, Stress and pore pressure histories in complex tectonic settings predicted with coupled geomechanical-fluid flow models: Marine and Petroleum Geology, doi:10.1016/j.marpetgeo.2016.03.031.

Oda, M., 1985, Permeability tensor for discontinuous rock masses: Geotechnique, doi:10.1680/geot.1985.35.4.483.

Sone, H., and M. D. Zoback, 2013, Mechanical properties of shale-gas reservoir rocks — Part 2: Ductile creep, brittle strength, and their relation to the elastic modulus: Geophysics, v. 78, no. 5, p. D393–D402, doi:10.1190/geo2013-0051.1.

Stephenson, B., E. Galan, M. Fay, A. Savitski, and T. Bai, 2018, Origin, detection, involvement in hydraulic stimulation and consequences for field development of large-scale structural lineaments in the marcellus and duvernay plays, *in* SPE/AAPG/SEG Unconventional Resources Technology Conference 2018, URTC 2018: doi:10.15530/urtec-2018-2902874.

Zhou, J., L. Zhang, X. Li, and Z. Pan, 2019, Experimental and modeling study of the stress-dependent permeability of a single fracture in shale under high effective stress: Fuel, doi:10.1016/j.fuel.2019.116078.

Zoback, M. D., and A. H. Kohli, 2019, Unconventional Reservoir Geomechanics: doi:10.1017/9781316091869.

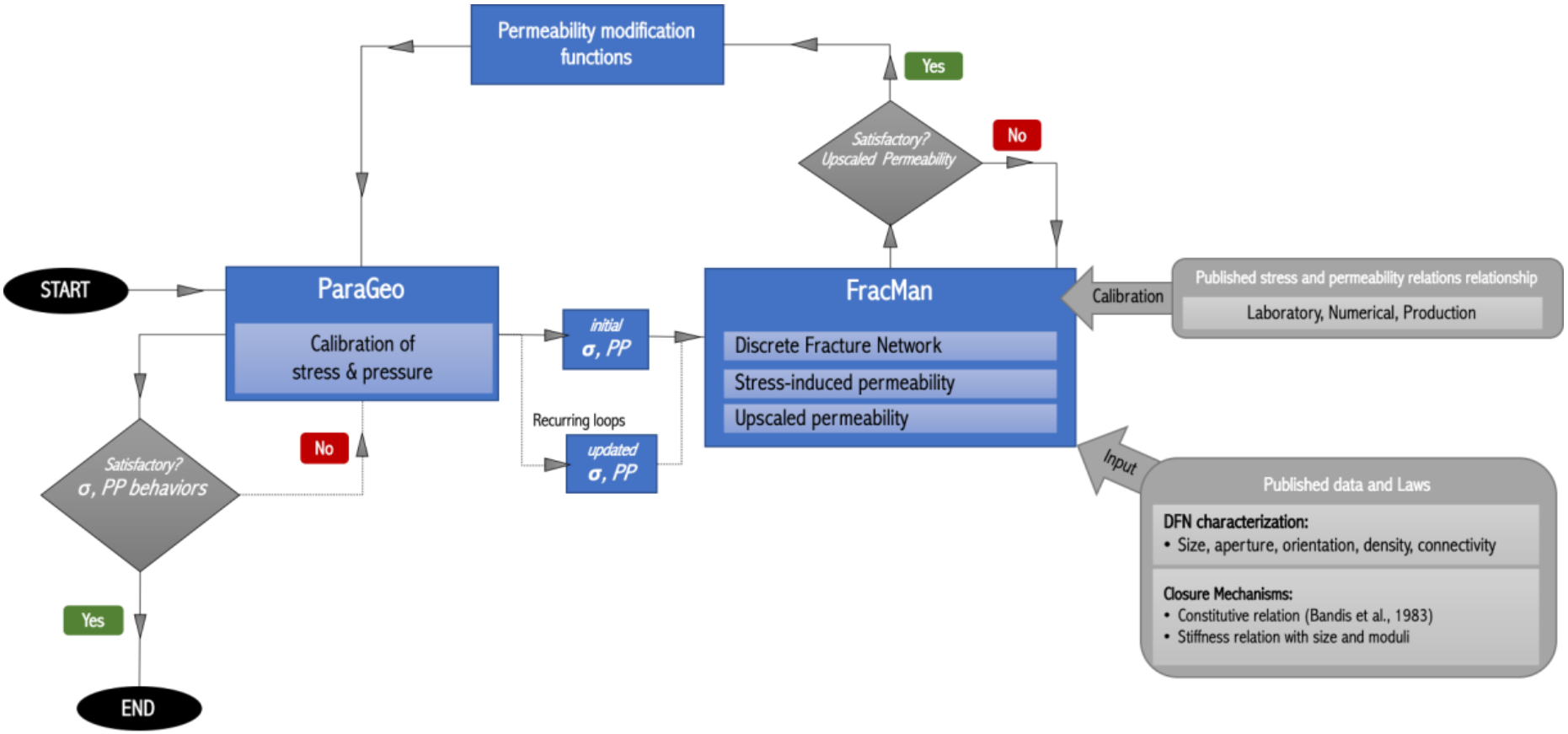

Figure 1. Proposed workflow showing feedback loops between ParaGeo's evolutionary stress and pressure and FracMan's upscaled permeability to derive permeability modification functions that satisfy realistic stress and pressure behaviors

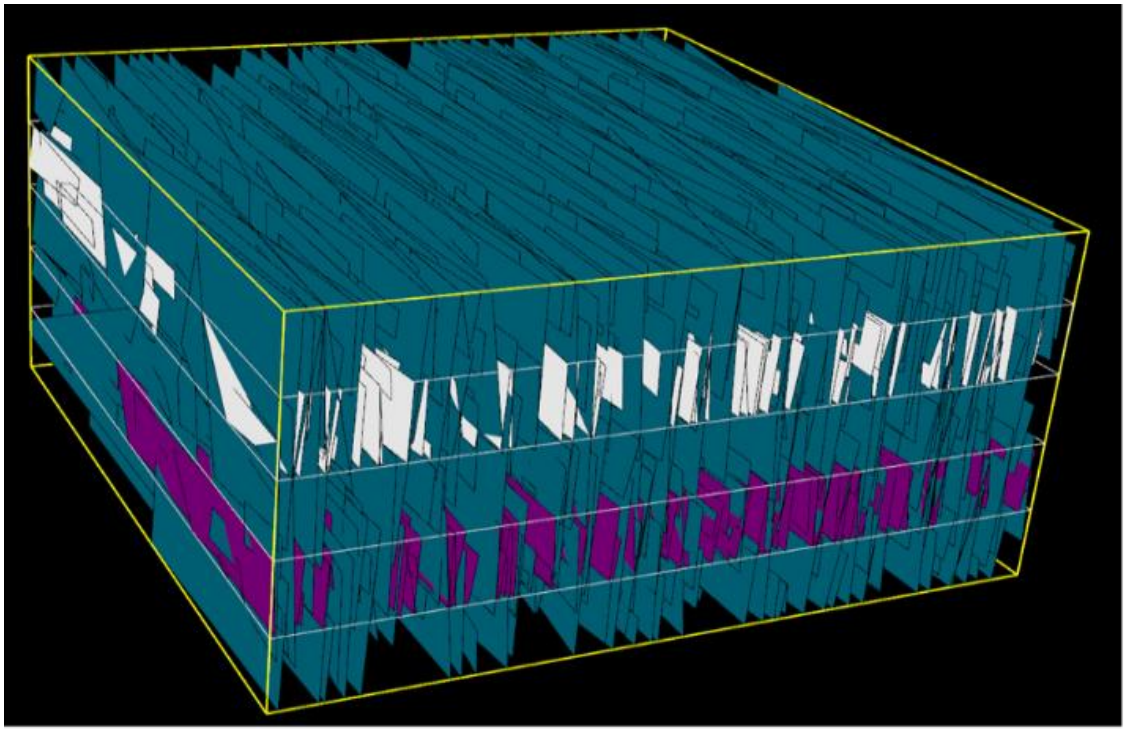

Fracture Characterization	Mean
Density (P32)	0.56 (m^2/m^3)
Frac_PORO	0.28%
Equivalent Radius (EQR)	14.3
Length (F_L)	46m
Height (F_H)	16m, 11m
Aperture	2.5mm
Fracture Permeability	900 mD

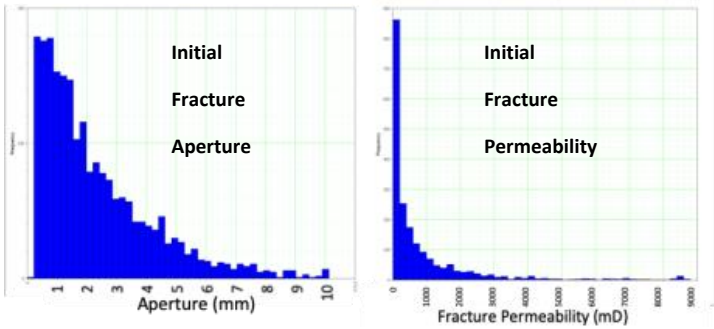

Figure 2. Target DFN with densely spaced, sub-vertical tensile fractures with bed-bound geometry built within FracMan and its characterization statistics (size, density, transmissivity).

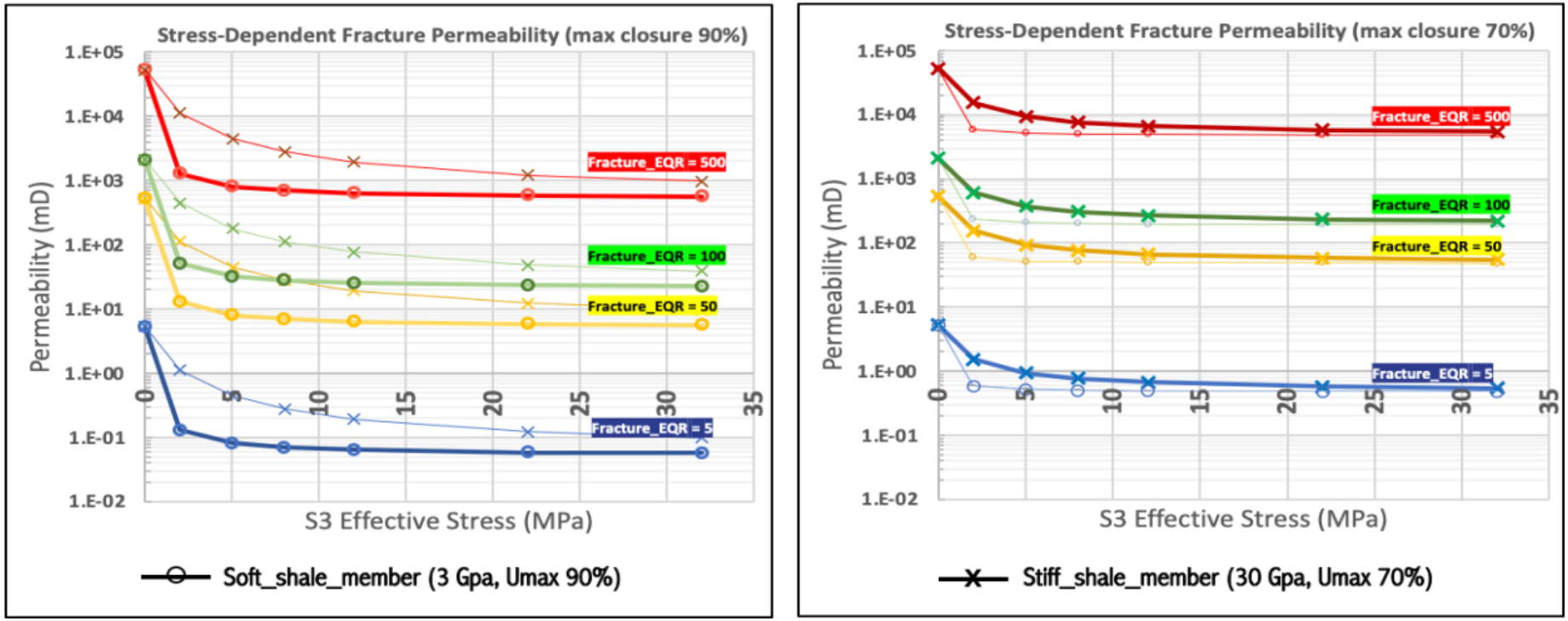

Figure 3. Stress-dependent fracture permeability under various maximum fracture closure and moduli assumptions. Thicken highlighted lines are the sets of soft and stiff shale members in various individual fracture sizes (5m-500m) for our analysis.

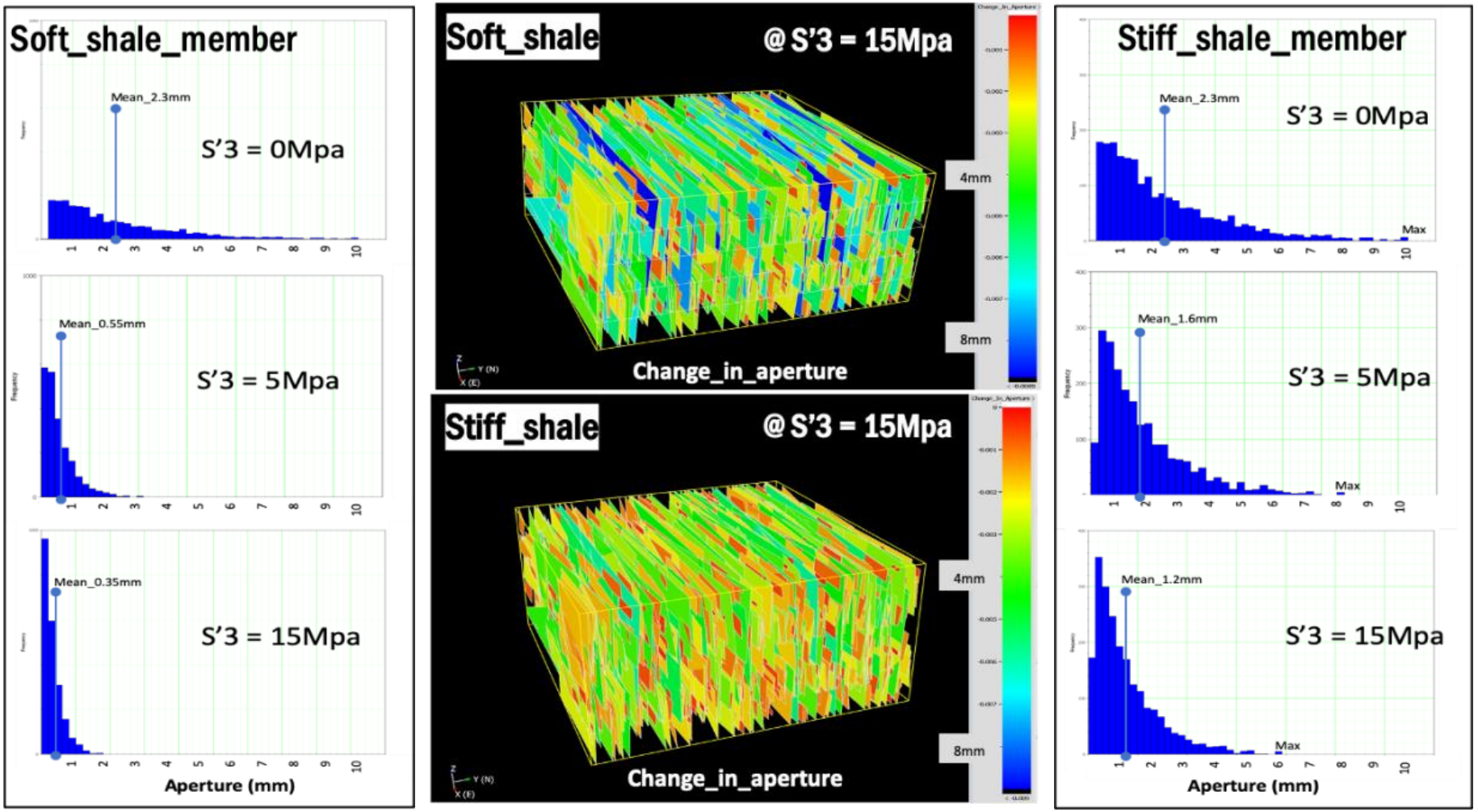

Figure 4. Evolution of fracture aperture closing under the applied effective stresses for Soft and Stiff shale members.

(A)

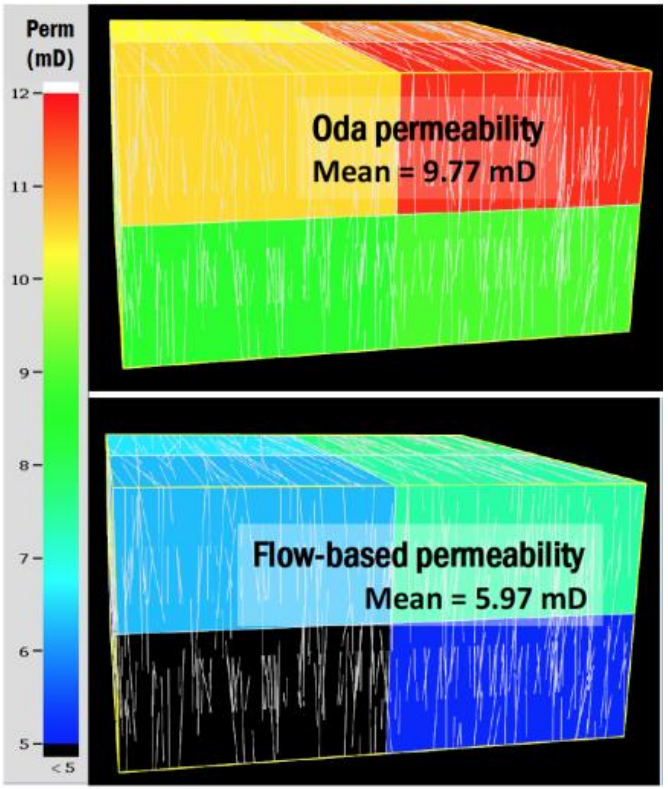

(B)

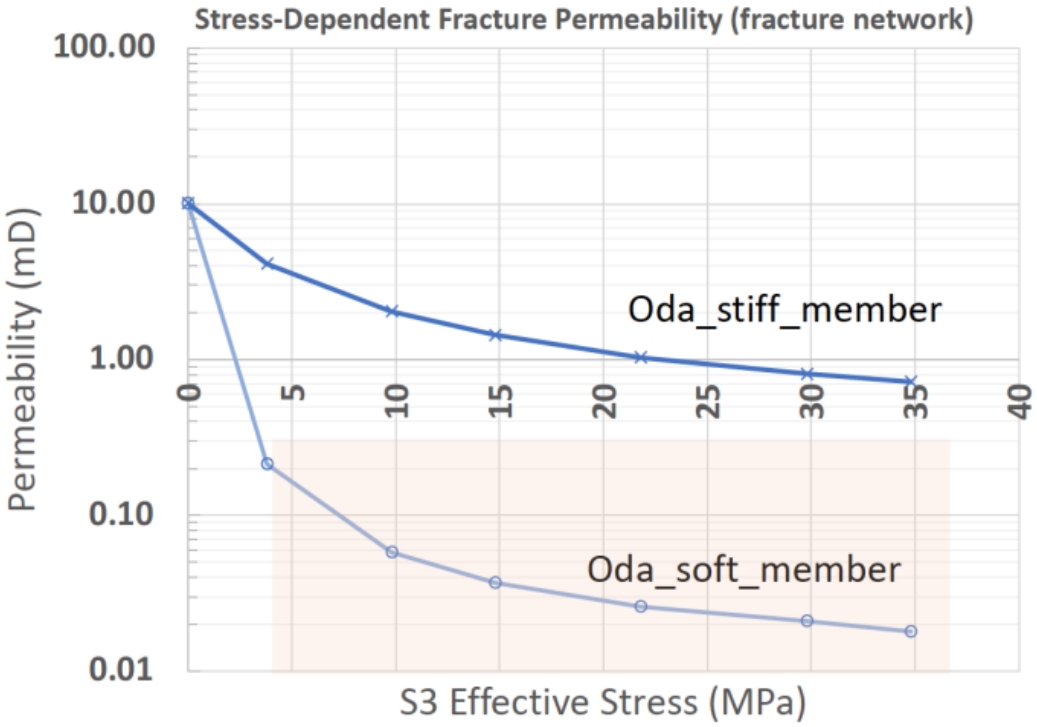

Figure 5. (A) Upscaled permeability for large element size suitable for basin-scale application. (B) Upscaled Oda permeability for stiff and soft shale endmembers.

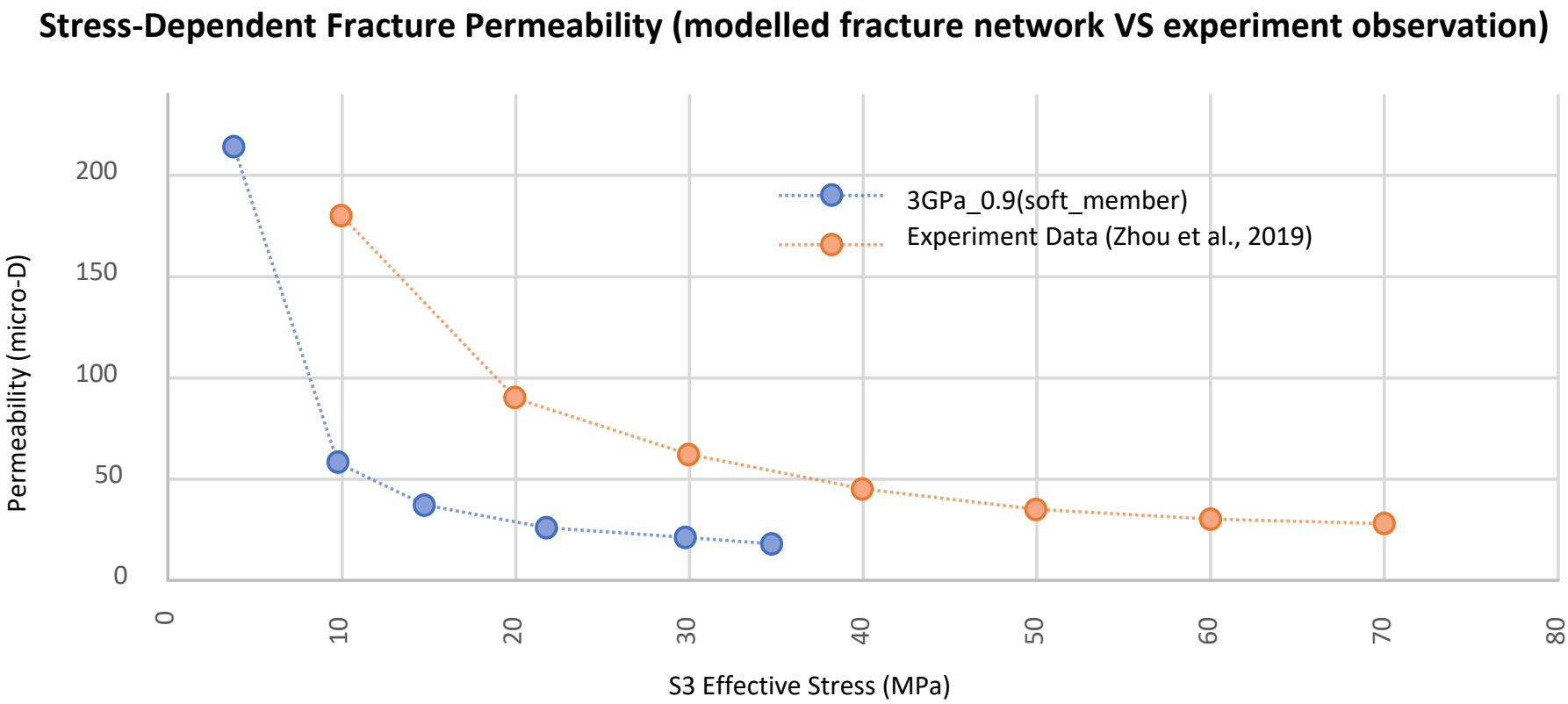

Figure 6. Permeability evolution for Oda_soft_member in this study compared to an observation from laboratory experiment (Zhou et al., 2019).

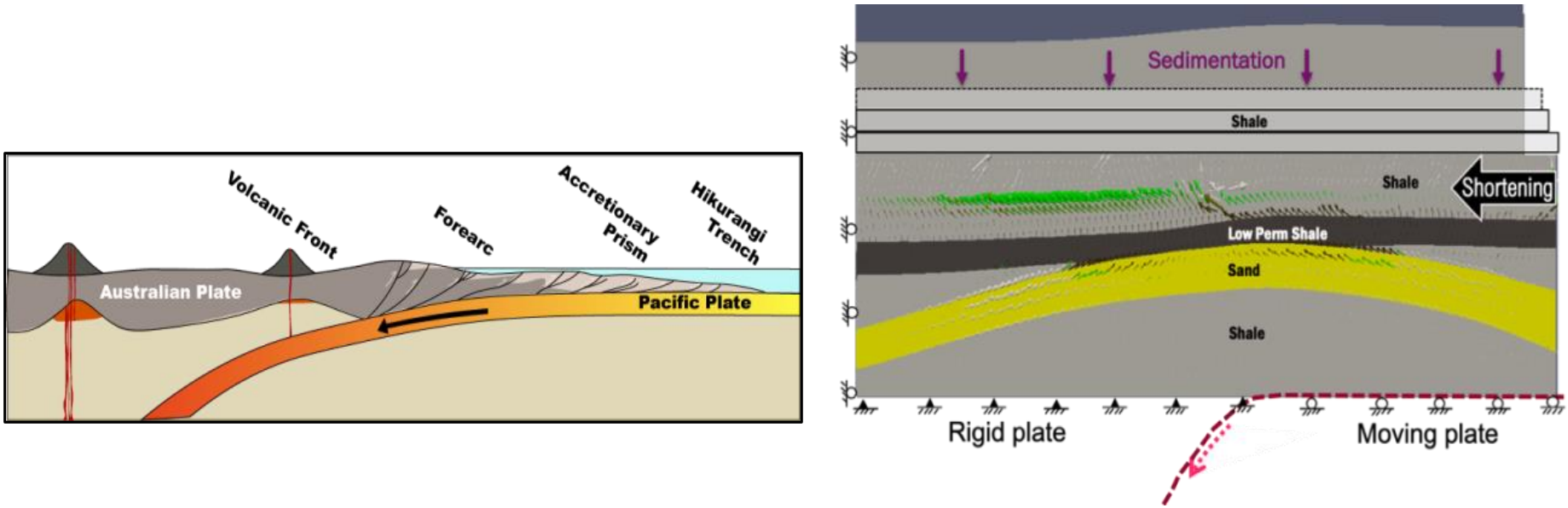

Figure 7. Comparison of complex structures overlying the Hikurangi Subduction Zone after Barnes et al. (2002) and the simplified synthetic model where the overpressured shale system is exposed to varying degrees of horizontal shortening and fracturing episodes over basin evolution.

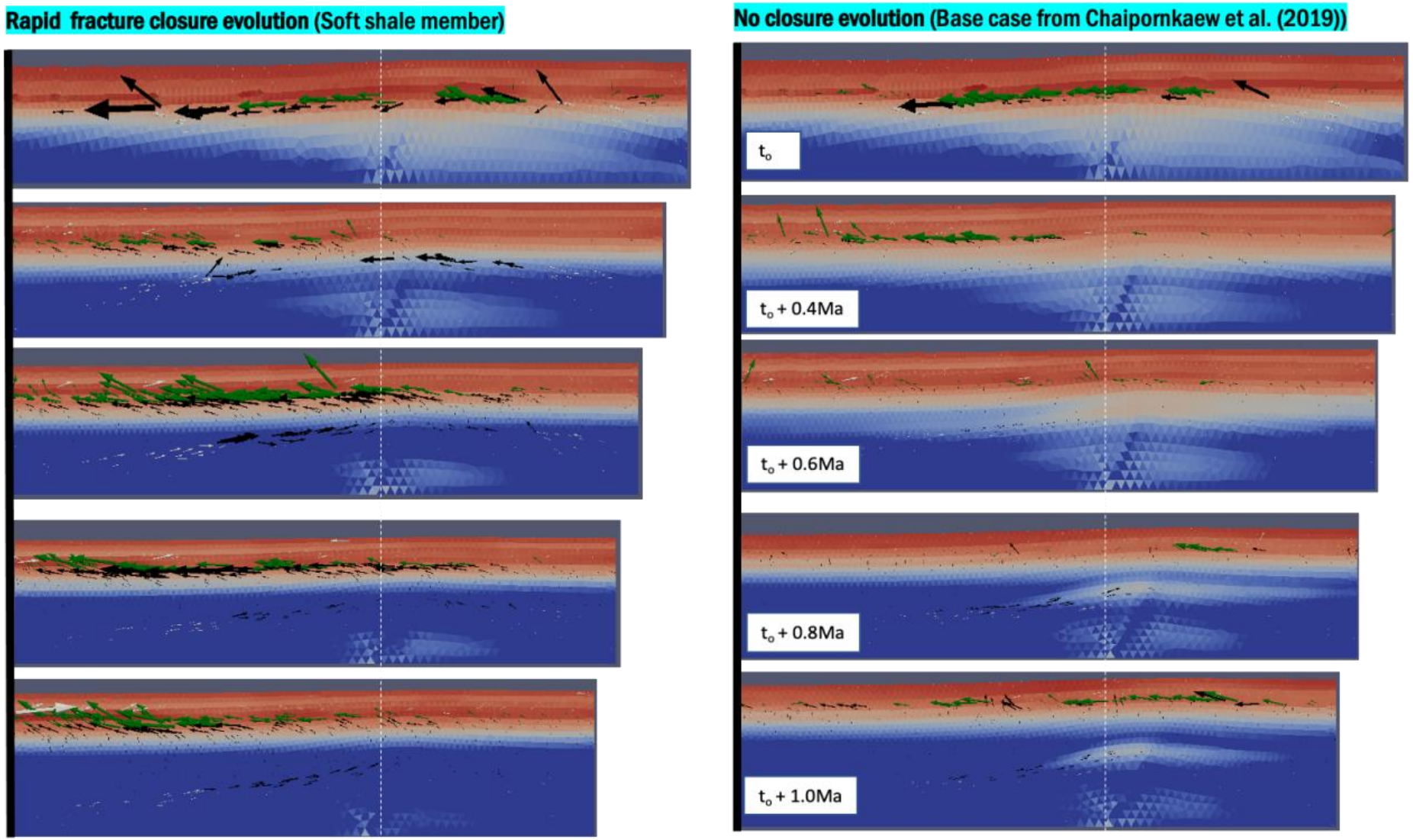

Figure 8. Comparison of two ParaGeo models with and without a rapid fracture closure evolution showing significant implication on pressure and stress accumulation over time.